Supporting Information

Self-assembly construction of a homojunction of Sn–Pb perovskite using an antioxidant for all-perovskite tandem solar cells with improved efficiency and stability

Zhuojia Lin[a], Jianwei Chen[a], Chenghao Duan[a], Kezhou Fan[b], Jiong Li[a], Shibing Zou[a], Feilin Zou[a], Ligang Yuan[c], Zheng Zhang[a], Kaicheng Zhang[d], Man Yu Lam[b], Sergeev A. Aleksandr[b], Jianhang Qiu[e], Kam Sing Wong[b], He Yan[f], Keyou Yan[a]*

[a] *School of Environment and Energy, State Key Laboratory of Luminescent Materials and Devices, Guangdong Provincial Key Laboratory of Solid Wastes Pollution Control and Recycling, South China University of Technology, Guangzhou, 510000, P. R. China.*

[b] *Department of Physics and William Mong Institute of Nano Science and Technology, The Hong Kong University of Science and Technology, Clear Water Bay, Kowloon 999077, Hong Kong, P. R. China.*

[c]*School of the Testing and Photoelectric Engineering, National Engineering Laboratory for Non-Destructive Testing and Optoelectronic Sensing Technology and Applications, Key Laboratory of Nondestructive Testing Ministry of Education, Nanchang Hangkong University, Nanchang 330063, China.*

[d]*Institute of Materials for Electronics and Energy Technology (i-MEET) Friedrich-Alexander-University Erlangen-Nuremberg Martensstraße 7, Erlangen 91058, Germany.*

[e]*Shenyang National Laboratory for Materials Science, Institute of Metal Research, Chinese Academy of Sciences, Shenyang, 110016, P. R. China.*

[f]*Department of Chemistry and Hong Kong Branch of Chinese National Engineering Research Center for Tissue Restoration and Reconstruction, Hong Kong University of Science and Technology, Clear Water Bay, Kowloon, Hong Kong 999077, China*

*To whom correspondence should be addressed.

E-mail: kyyan@scut.edu.cn

Experimental Methods

Materials: Poly(3,4-ethylenedioxythiophene):poly(styrenesulfonate) (PEDOT:PSS) (aqueous dispersion, Clevios VP AI 4083) was obtained from Heraeus. Cesium iodide (CsI, 99.9%), Tin difluoride (SnF_2, 99%), N,N-dimethylformamide (DMF, anhydrous, 99.8%), isopropanol (IPA, anhydrous, 99.8%), Dimethyl sulfoxide (DMSO, anhydrous, ≥ 99.9%), Anisole (anhydrous, 99%) and Chlorobenzene (CB, anhydrous, 99.8%) were purchased from Sigma-Aldrich. Lead iodide (PbI_2, 99.99%), lead bromide ($PbBr_2$, 99.99%), 1,3-Propyldiammonium diiodide($PDAI_2$, 99.5%) and C_{60} (99%) were all purchased from Xi'an Polymer Light Technology Corporation. Nickel oxide (NiO_x) nanoparticles，Indium tin oxide (ITO) and Tin diiodide (SnI_2, 99.99%) were obtained from Advanced Election Technology Co., Ltd. [4-(3,6-Dimethyl-9H-carbazol-9-yl)butyl]phosphonic Acid (Me-4PACz) were purchased from Tokyo Chemical Industry Co., Ltd. (TCI). 4-(Trifluoromethyl)phenylhydrazine hydrochloride(TFPHCl, 96%) was obtained from Alfa Aesar. Indene-C_{60} bisadduct (> 99%) was purchased from 1-materia. Tetrakis(dimethylamino)tin(IV) was purchased from Nanjing ai mou yuan Scientific equipment Co.. Ltd. All solvents and chemicals were purchased commercially and used as received without further purification. Silver particles were purchased from Zhongnuo Advanced Material (Beijing) Technology Co., Ltd.

Single-junction NBG perovskite solar cells fabrication: The patterned ITO substrates were cleaned by serial ultrasonic cleaning with, acetone, deionized water, and isopropanol for 15 min. The PEDOT:PSS solution was spin-coated onto the ITO substrate for 30 s at 4000 rpm following the UV ozone treatment for 15 min and then

annealed for 20 min at 150 °C. For preparing 1.9 M precursor solutions of NBG perovskite, FAI, CsI, MAI, PbI_2, SnI_2, SnF_2, NH_4SCN with molar ratio of 0.6:0.1:0.3:0.9:0.9:0.1:0.03 and a certain amount of TFPHCl additive were dissolved in a mixed solvent of 750 μL DMF and 250 μL DMSO. For the deposition of NBG perovskite films, the deposition process was performed in two steps: (1) 1,000 rpm for 10 s at an acceleration of 200 rpm s^{-1} and (2) 4,000 rpm for 40 s at an acceleration of 1,000 rpm s^{-1}; 350 μl of CB was dropped rapidly at 20 s before the second step of the spin-coating process was completed. Finally, 30 nm of C_{60}, 8 nm of BCP and 100 nm of Ag were deposited sequentially to complete the preparation of single-junction NBG device with an active area of 0.0525 cm^2.

Rich-Sn NBG perovskite solar cells fabrication: The patterned ITO substrates were cleaned by serial ultrasonic cleaning with, acetone, deionized water, and isopropanol for 15 min. The PEDOT:PSS solution was spin-coated onto the ITO substrate for 30 s at 4000 rpm following the UV ozone treatment for 15 min and then annealed for 20 min at 150 °C. For the preparation of Rich-Sn $FA_{0.6}MA_{0.3}Cs_{0.1}Pb_{0.4}Sn_{0.6}I_3$ precursor solution, FAI, CsI, MAI, PbI_2, SnI_2, SnF_2, NH_4SCN with molar ratio of 0.6:0.1:0.3:0.72:1.08:0.1:0.03 and a certain amount of TFPHCl additive were dissolved in a mixed solvent of 750 μL DMF and 250 μL DMSO. For the deposition of NBG perovskite films, the deposition process was performed in two steps: (1) 1,000 rpm for 10 s at an acceleration of 200 rpm s^{-1} and (2) 4,000 rpm for 40 s at an acceleration of 1,000 rpm s^{-1}; 350 μl of CB was dropped rapidly at 20 s before the second step of the spin-coating process was completed. Then, perovskite films were annealed at 100°C for

10 min. Finally, 30 nm of C_{60}, 8 nm of BCP and 100 nm of Ag were thermally deposited sequentially to complete the preparation of rich-Sn NBG devices.

Sn pure NBG perovskite solar cells fabrication: The patterned ITO substrates were cleaned by serial ultrasonic cleaning with, acetone, deionized water, and isopropanol for 15 min. The PEDOT:PSS solution was spin-coated onto the ITO substrate for 30 s at 4000 rpm following the UV ozone treatment for 15 min and then annealed for 20 min at 150 °C. For the preparation of Sn pure $(FA_{0.9}EA_{0.1})_{0.98}EDA_{0.01}SnI_3$ precursor solution, FAI, EAI, $EDAI_2$, SnI_2, SnF_2, NH_4SCN with molar ratio of 0.882:0.098:0.01:1:0.1:0.03 and a certain amount of TFPHCl additive were dissolved in a mixed solvent of 750 μL DMF and 250 μL DMSO. The precursor solution were spun on the ITO/PEDOT:PSS substrates at 5000 rpm for 30 s. 150 mL CB as the anti-solvent was dropped at the 9th sec after spinning started and the films were annealed at 90 °C for 10 min. Next, ICBA (18 mg/mL in CB) solution was spin-coated at 4000rpm for 30 s and annealed at 70 °C for 5 min. Finally, 8 nm of BCP and 100 nm of Ag were thermally deposited sequentially to complete the preparation of Sn pure NBG devices under a vacuum of 3.0×10^{-4} Mbar.

Preparation of ALD SnO_2: ALD deposition instruments purchased to Beijing Antechnology Co.,LTD. Tetrakis(dimethylamino)tin(IV) (TDMASn) (at 55 °C) and H_2O (at 25 °C) were used as precursors for SnO_2 growth. Nitrogen as carrier gas and process flow rates was set to 150 sccm. SnO_2 growth consisted of a cyclical process of the TDMASn dose (0.35 s), a purge (20 s), a water dose (0.5 s) and a purge (20 s). SnO_2

film with a thickness of 70 nm needed 400 cycles.

All-perovskite tandem solar cells fabrication: First, NiOx nanocrystals (20 mg/mL in water) were spin-coated on an ITO substrate at 3,000 rpm for 30 s and then annealed in air on a hot plate at 130 °C for 30 min. The 0.3 mg/mL Me-4PACz solution (in ethanol) was spin-coated onto the ITO/NiOx substrate at 3000 rpm for 30s and followed by annealing at 100 °C for 10 min. The WBG precursor solution was prepared by dissolving FAI, CsI, PbI_2, and $PbBr_2$ with molar ratio of 0.8:0.2:0.4:0.6 in a mixed solvent of DMF and DMSO with a volume ratio of 4:1. The WBG precursor solution were spun on the ITO//NiOx/Me-4PACz substrate at 5000 rpm for 30 s, 100 mL Anisole as anti-solvent was dropped at 8 seconds before the end of the spin-coating, and annealed at 100 °C for 10 min. Then, $PDAI_2$ dissolved in IPA (1 mg/mL) was spin-coated onto the WBG perovskite surface at 4000 rpm for 40 s and followed by annealing at 100 °C for 5 min. Upon cooling to room temperature, both the 20 nm thick C_{60} film and the 70 nm thick SnO_2 layer were deposited by thermal evaporation and ALD. Then, 1 nm of Au was deposited as a recombination-layer by thermal evaporation. At last, the above single-junction NBG device procedure was duplicated to finalize all perovskite tandem solar cells.

Films characterization

Thermo Scientific ESCA Lab 250Xi was employed to test X-ray photoelectron spectroscopy (XPS) of NBG perovskite films coated on glass substrates. Curve fitting was performed using Avantage software and was corrected based on the C1s peak at 284.8 eV. The morphologies of perovskite films and corresponding devices, and

energy-dispersive X-ray spectroscopic (EDX) were measured by scanning electron microscope (Zeiss Merlin). EDX measurements: low operating voltages (< 20 kV), low beam current (500 pA) and short exposure time (≈ 2 min). Nanomeasurer 1.2 software were used for statistical analysis of size distributions. Fourier transform infrared spectroscopy (FTIR) were carried out by Nicolet 6700. Atomic force microscopy (AFM) and Kelvin Probe Force Microscopy (KPFM) measurements were carried out by NT-MDT Ntegra Prima. AFM and KPFM images were processed using software Gwyddion Analysis. The steady state photoluminescence (PL) and time-resolved photoluminescence (TRPL) spectra were recorded by FLS1000 (Edinburgh Instrument, UK). NBG perovskite films were excited by a picosecond pulsed laser with a wavelength of 680 nm and excitation frequency of 10 kHz. UV-visible (UV-Vis) spectra was performed on UV-vis-NIR Spectrophotometer of UV3200. UPS was performed with a photoelectron spectroscopy system (PHI5000 VersaProbe III) with He I excitation (21.22 eV). A -10 V bias was applied to samples of NBG perovskite films. X-ray diffraction (XRD) and X-ray diffraction (GIXRD, at a small diffraction angle (0.3°)) for perovskite films were measured on Empyrean diffractometer with regions of 5-50°. The contact angle has been recorded at a Krüss DSA100s drop shape analyzer. The scanning PL mapping measument employed a custom-built laser scanning confocal microscope set-up with photon counter module. Excitation was achieved using a He-Ne laser (635 nm) with adjustable power modulated via neutral density (ND) filters. Photon counting data from counter module was collected and analysed by our home-built labview software. Samples of NBG perovskite for XPS, UV-Vis, XRD, UPS, SEM, EDX, contact angle, AFM and KPFM measurement fabricated on glass/ITO. For TRPL spectra: glass/NBG perovskite, glass/PEDOT:PSS/NBG perovskite and glass/NBG perovskite/C_{60}.

Device characterization

J-V characteristics of PSCs were taken using a Keithley 2400 source measurement unit under a simulated AM 1.5G spectrum. With a SS-F5-3A solar simulator (Enli

Technology CO., Ltd.), the light intensity was calibrated by standard single-crystal silicon solar cells (KG5). *J-V* curves were all measured in Ar-filled glovebox with a scanning rate of 100 mV s^{-1} (with voltage steps of 20 mV and a delay time of 100 ms. Current-voltage (I-V) curves of electron-only devices was measured by using a Keithley 2400 Source Meter under dark condition. The incident photon-to-electron conversion efficiency (IPCE) spectra were detected on monochrome illumination (Oriel Cornerstone 260 1/4 m monochromator with Oriel 70613NS QTH lamp) and the incident light was calibrated by a monocrystalline silicon diode. Electrical impedance spectroscopy (EIS) and Mott-Schottky plot were obtained by an IM6 electrochemical workstation (Zahner Zennium, Germany) at room temperature in ambient conditions. Ultrafast transient absorption (TA) spectroscopy were analyzed on semi-devices consisting of NBG perovskite films intercalated between PEDOT:PSS and C_{60}. Excitation pump pulses at 400 nm was generated by splitting the fundamental pulse into an optical parametric amplifier (Opera Solo).

Long-term stability measurements: For the long-term storage stability (w/o and with heated aging), unencapsulated devices with Ag metal electrode were stored at Ar filled glovebox under dark condition. For air stability, unencapsulated devices with Ag metal electrode were stored at 25 °C with 30% humidity. Photostability was measured with a white light-emitting diode (LED) lamp under MPP tracking in an Ar-filled glove box at 25°C (purchased from Guangzhou Crysco Equipment Co., Ltd), and the radiation intensity is adjusted according to the current density of PSCs, which is equal to the J_{SC} under the solar simulator. Ag metal electrode in NBG and tandem devices were replaced by Au metal electrode to measure photostability. Additionally, device stability measurements in terms of storability, photostability, thermo-stability and humidity-stability were presented based on an average of 5 devices.

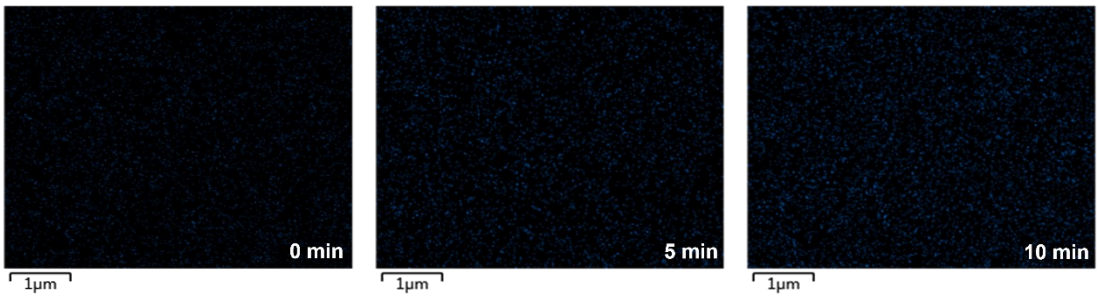

Figure S1. EDX mapping of fluorine for top surface of NBG perovskite films at different annealing time.

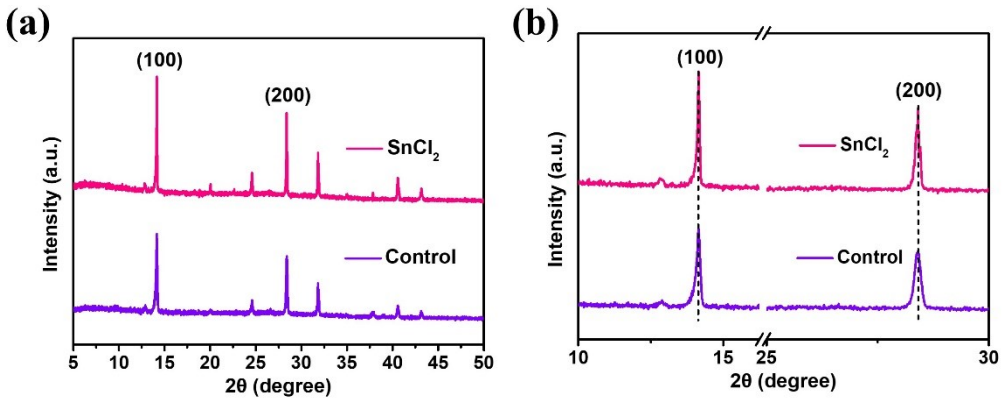

Figure S2. (a) XRD spectra of NBG perovskite films prepared w/o and with $SnCl_2$. (b) corresponding zoomed-in patterns in the regions of 10-30°.

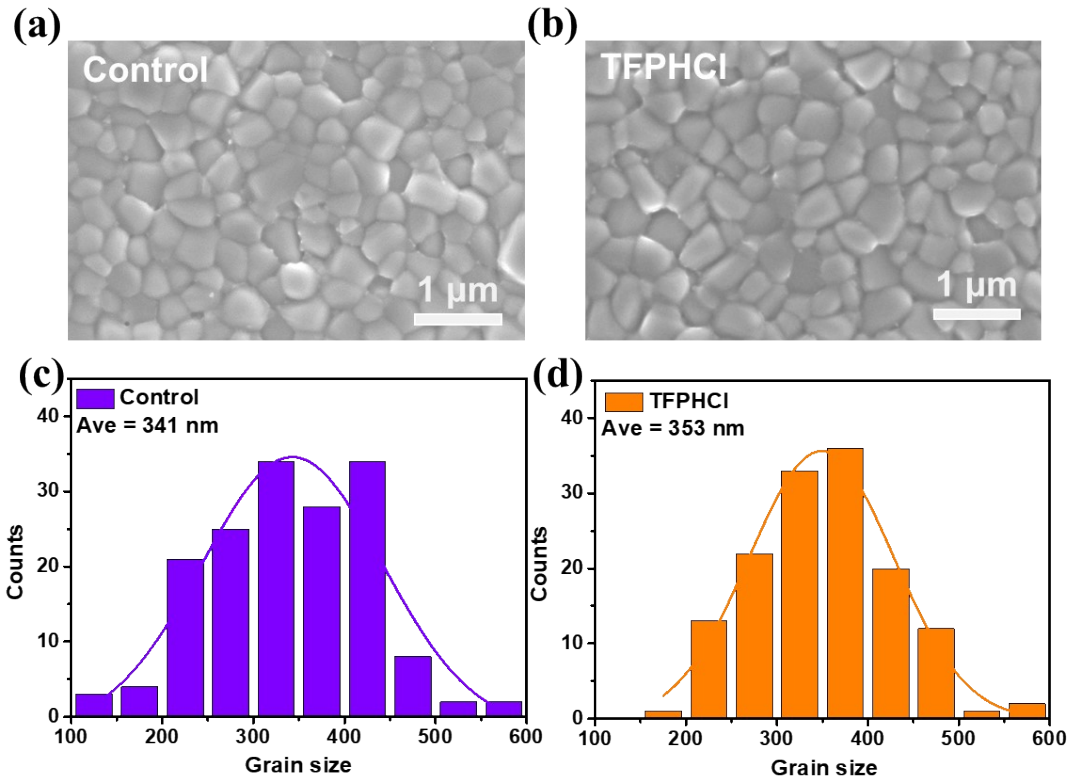

Figure S3. SEM images and grain size distribution of NBG perovskite films prepared (a, c) w/o and (b, d) with TFPHCl.

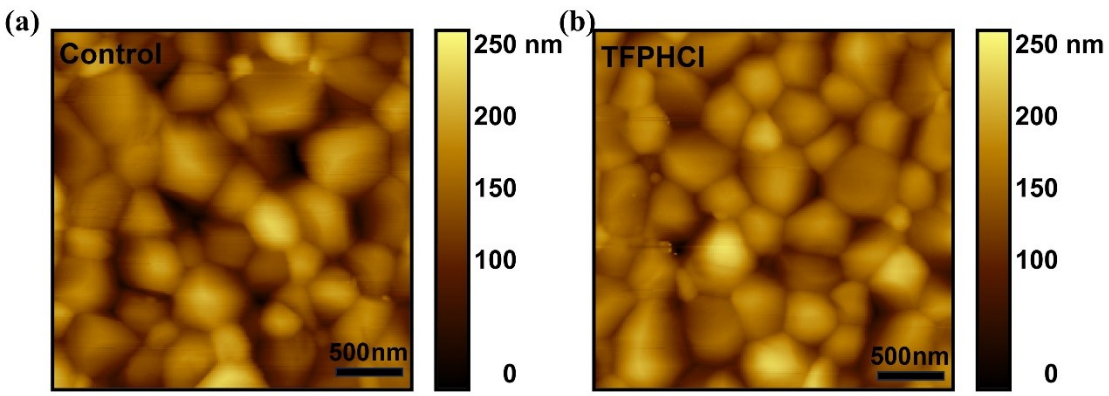

Figure S4. AFM images of NBG perovskite films prepared (a) w/o and (b) with TFPHCl.

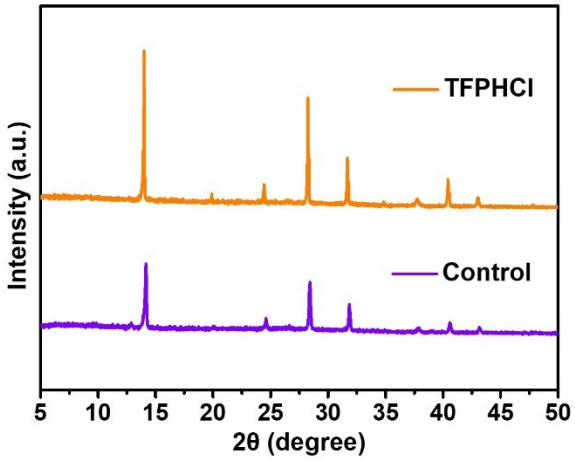

Figure S5. XRD spectra of NBG perovskite films prepared w/o and with TFPHCl.

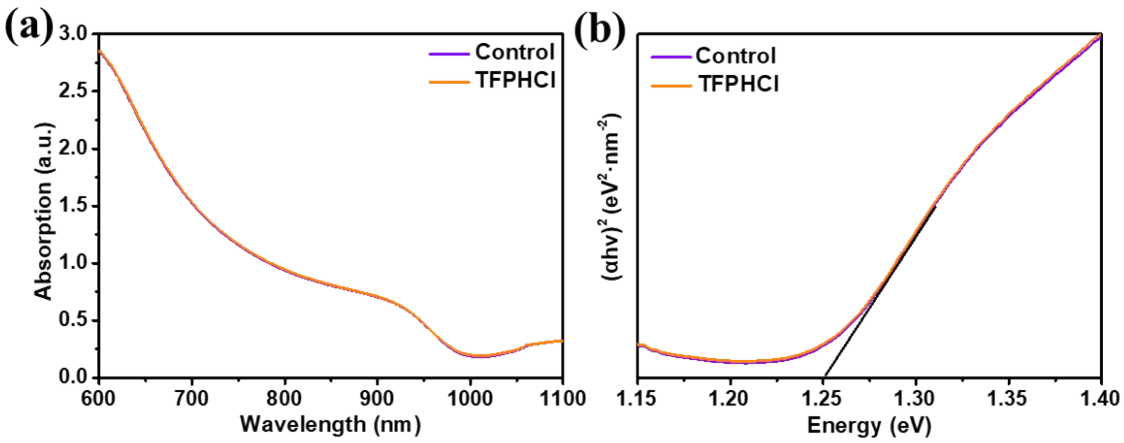

Figure S6. (a) UV-Vis absorption spectra and (b) relationship of $(\alpha h\nu)^2$ vs energy for NBG perovskite films w/o and with TFPHCl.

$$(\alpha h\nu)^{\frac{1}{2}} = B(h\nu - E_g) \quad (1)$$

α, B, h, ν are absorption coefficient, constant, Planck constant, incident photon frequency, respectively[1]. Eg represents bandgap of NBG perovskite. An approximate straight line can be located on the curve and extended to the x-axis, and its intersection with x-axis was Eg of NBG perovskite.

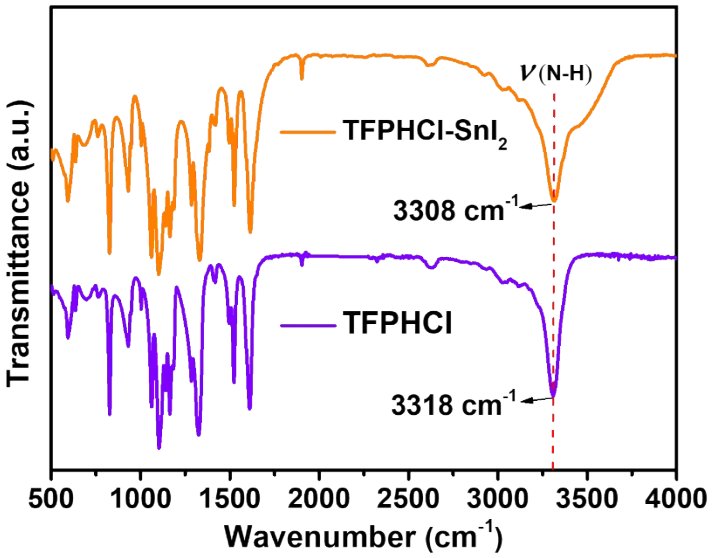

Figure S7. FTIR spectra of TFPHCl and TFPHCl-SnI_2.

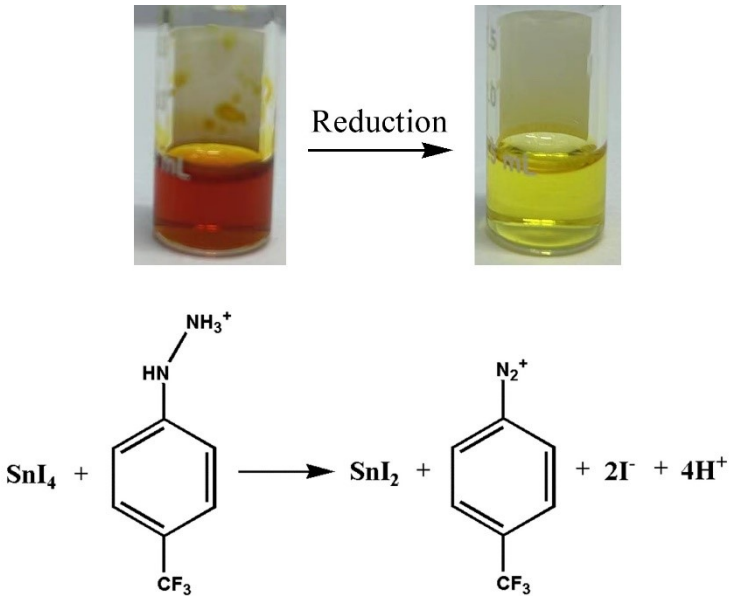

Figure S8. Photographs of SnI_4 and SnI_4-TFPHCl solutions after stirring and corresponding chemical reaction for restoring Sn^{4+} back to Sn^{2+}.

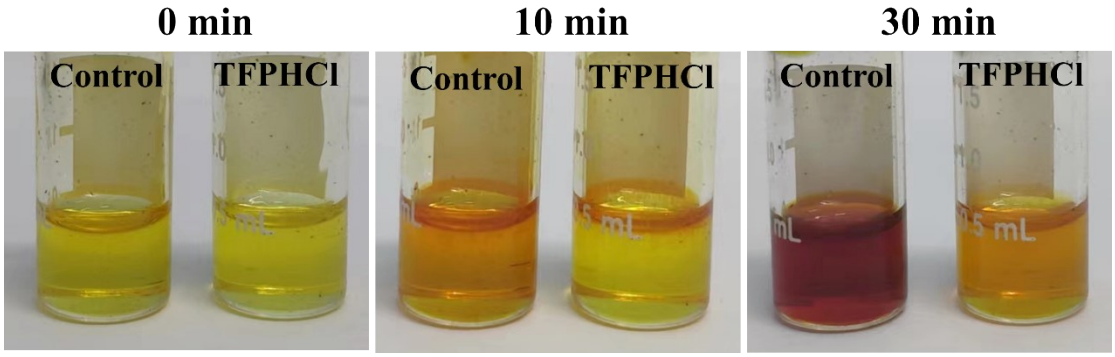

Figure S9. Images of SnI_2 solution w/o and with TFPHCl as a function of increasing exposure time to air.

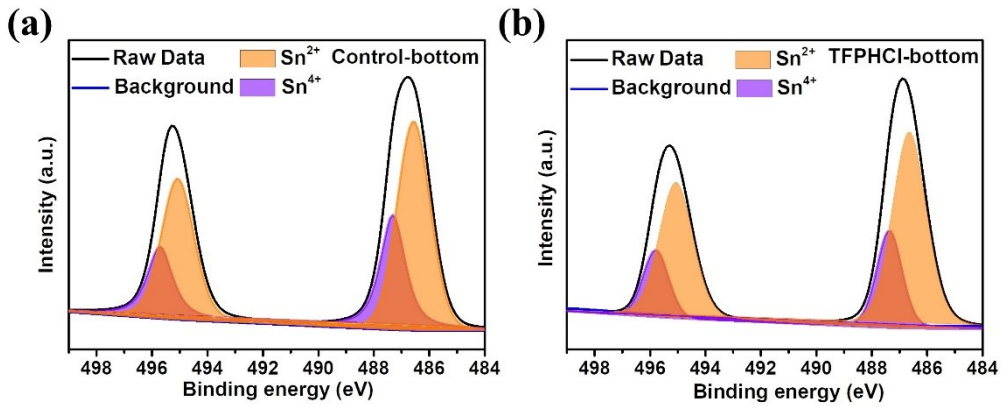

Figure S10. (a, b) Sn 3d XPS spectra for bottom surfaces of NBG perovskite films w/o and with TFPHCl.

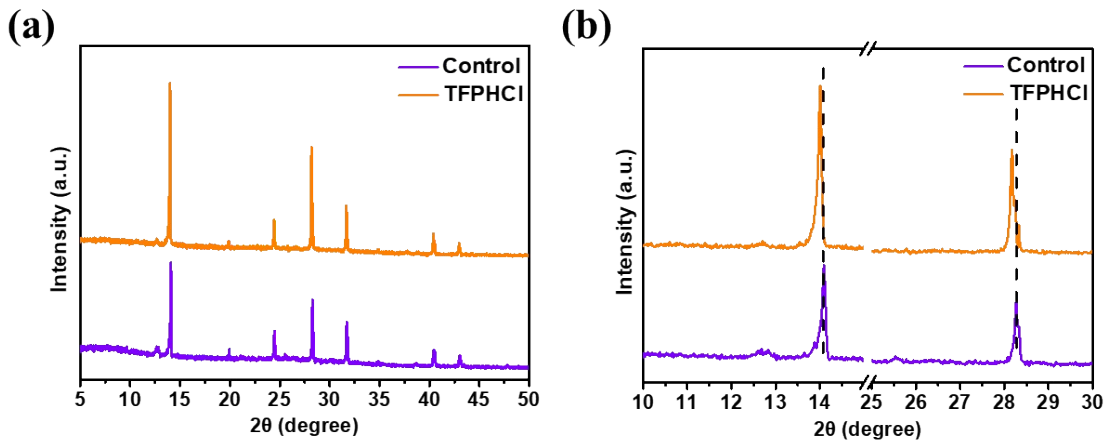

Figure S11. (a) GIXRD spectra of NBG perovskite films prepared w/o and with TFPHCl. (b) corresponding zoomed-in patterns in the regions of 10-30°.

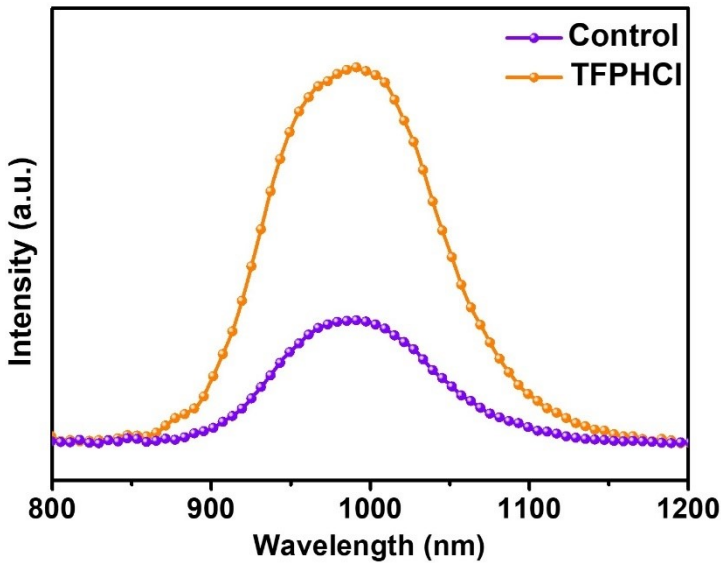

Figure S12. PL spectrum of NBG perovskite films prepared w/o and with TFPHCl.

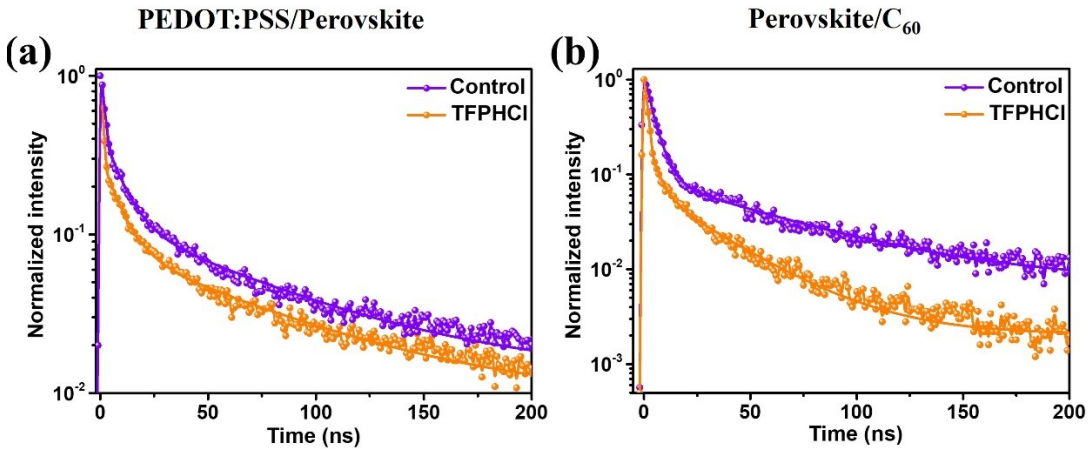

Figure S13. Time-resolved PL decay spectra of NBG perovskite films w/o and with TFPHCl featuring (a) hole (PEDOT:PSS) or (b) electron (C_{60}) extraction layers.

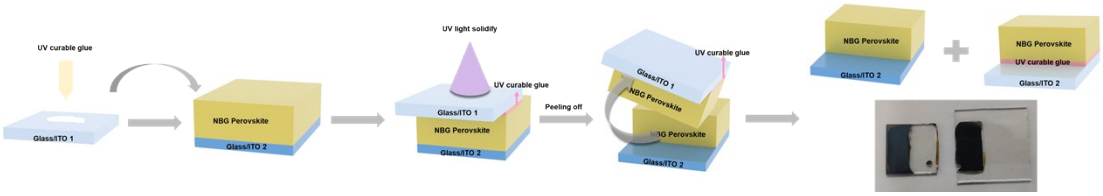

Figure S14. Schematic diagram of exposing bottom surface and corresponding experimental photographs. Firstly, small amount of conductive UV curable glue ((nondestructive to NBG perovskite film) was dropped on a clean glass/ITO substrate 1. Then, glass/ITO substrate 1 was covered with the top surface of NBG perovskite films/ITO/glass substrate 2. Glass/ITO substrate 1 was stressed so that a tight contact between conductive UV curable glue and NBG perovskite film was achieved, and was solidified using ultraviolet light. Finally, UV curable glue coated glass/ITO was forcefully peeled off from underlying glass/ITO substrate 2, and NBG perovskite film was completely separated from underlying glass/ITO substrate 2 and transferred to glass/ITO substrate 1. When turned over on the glass/ITO substrate 2, the bottom surface of NBG perovskite film was fully exposed and various characterisations could be performed on it.

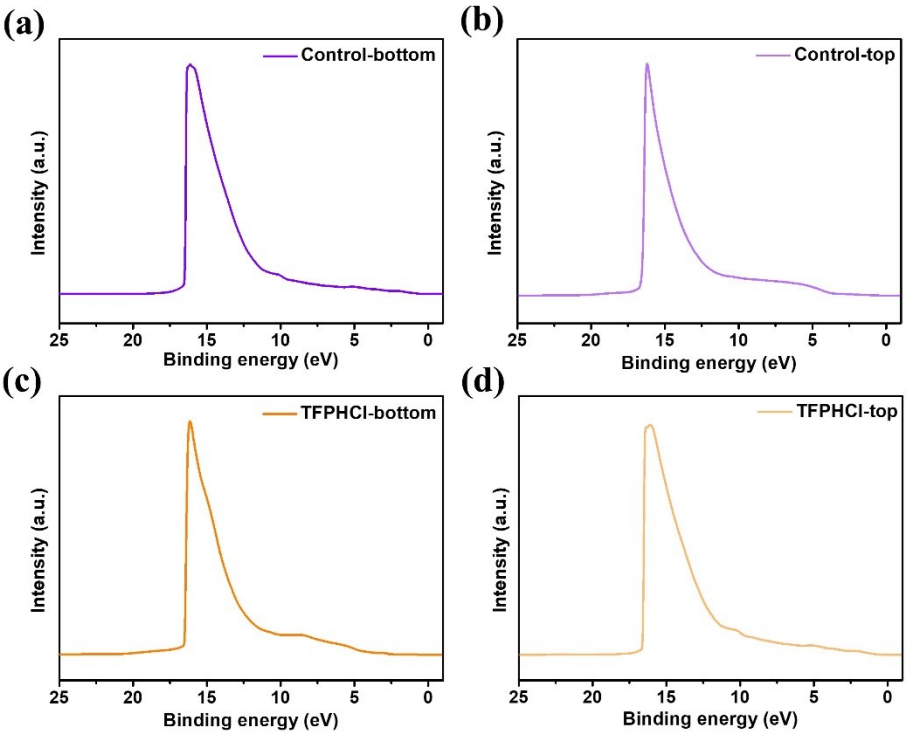

Figure S15. Full UPS spectra for NBG perovskite films after energy calibration.

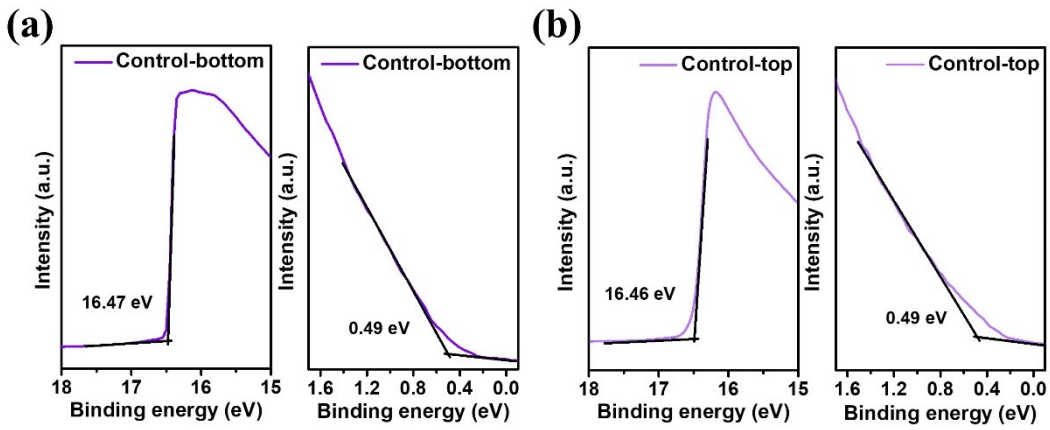

Figure S16. UPS spectra of (b) top and (c) bottom surfaces in NBG perovskite films w/o TFPHCl. The secondary electron cutoff energy (E_{Cutoff}) and onset (E_{Onset}) energy were obtained by following method from UPS spectrum.

E_{Cutoff}: linear fit and linear extrapolation of steeply descending portion along the secondary electron cut-off edge, and taking the intersection with the background noise baseline.

E_{Onset}: linear fit and linear extrapolation of steeply descending portion along starting edge in the valence band spectrum, and taking intersection with the background noise baseline.

E_F, E_{VBM} and E_{CBM} were calculated by following formula[2-4]:

$$E_F = E_{Cutoff} - 21.22\ eV \quad (2)$$

$$E_{VBM} = E_F - E_{Onset} \quad (3)$$

$$E_{CBM} = E_{VBM} - E_g \quad (4)$$

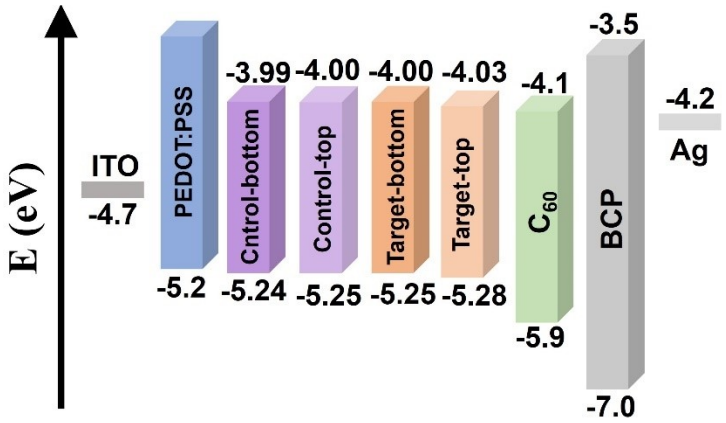

Figure S17. Energy-level diagram of NBG device.

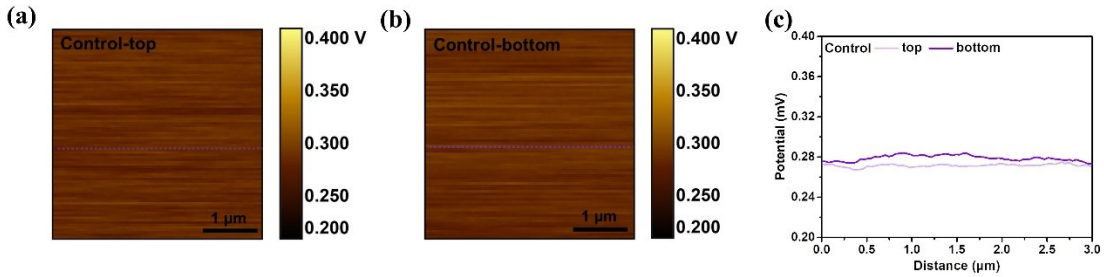

Figure S18. KPFM images of (a) top and (b) bottom surfaces for NBG perovskite films w/o TFPHCl, and (c) corresponding surface potential curve captured on the horizontal line marked in (a) and (b).

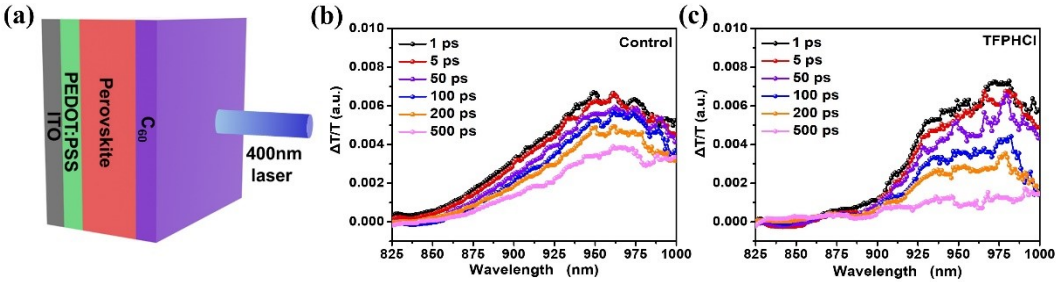

Figure S19. (a) Schematic of device structure (ITO/PEDOT:PSS/NBG perovskite/C_{60}) utilized for TA measurements using a 400 nm pump pulse generated by a fs laser. The delay time-dependent TA spectra of (b) control and (c) TFPHCl-modified NBG semi-devices.

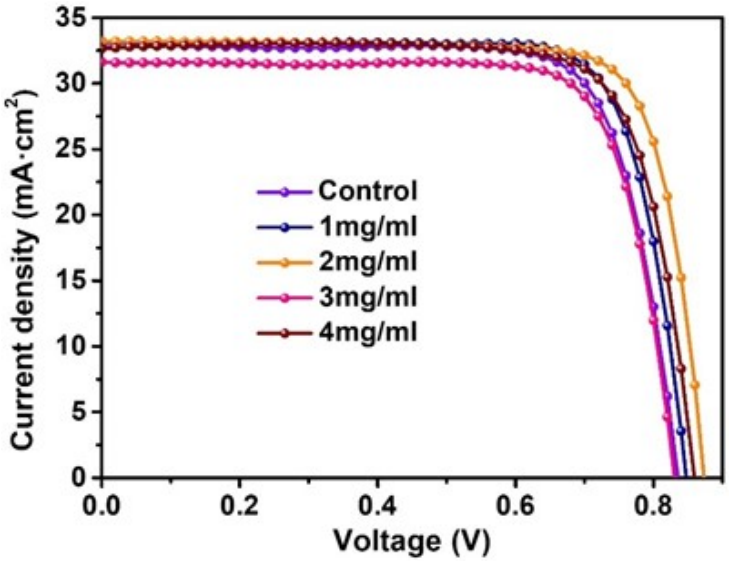

Figure S20. *J-V* curves of NBG devices with different concentration TFPHCl.

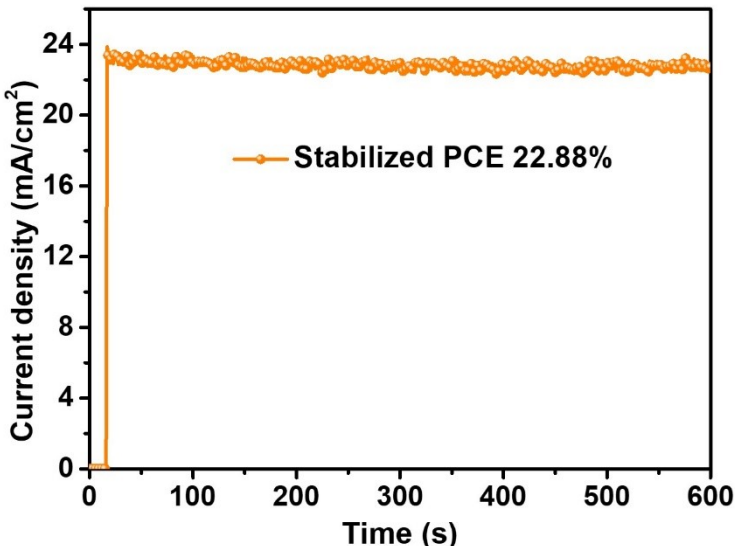

Figure S21. Steady-state output PCE of TFPHCl-modified NBG device at the maximum power point of 0.76 V.

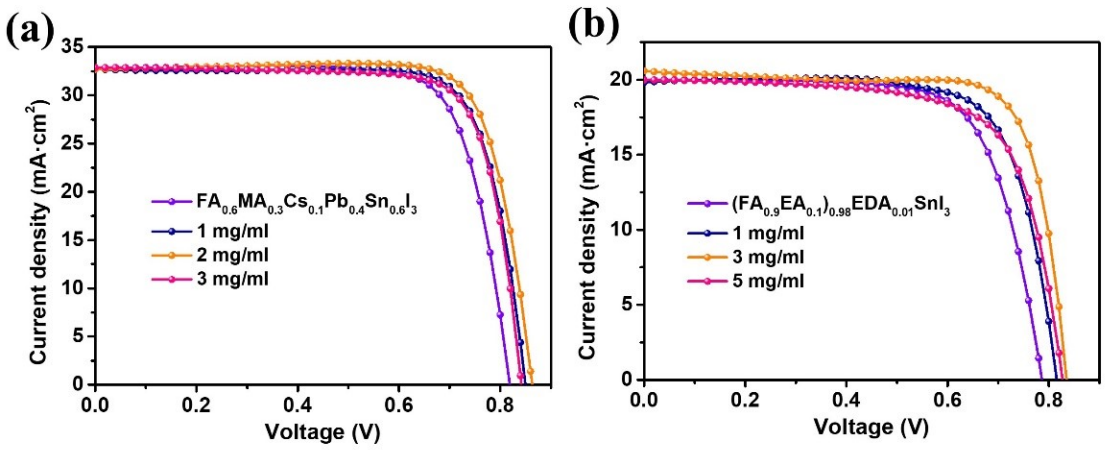

Figure S22. *J-V* curves of NBG devices of (a) $FA_{0.6}MA_{0.3}Cs_{0.1}Pb_{0.4}Sn_{0.6}I_3$ and (b) $(FA_{0.9}EA_{0.1})_{0.98}$ $EDA_{0.01}SnI_3$ with different concentration TFPHCl.

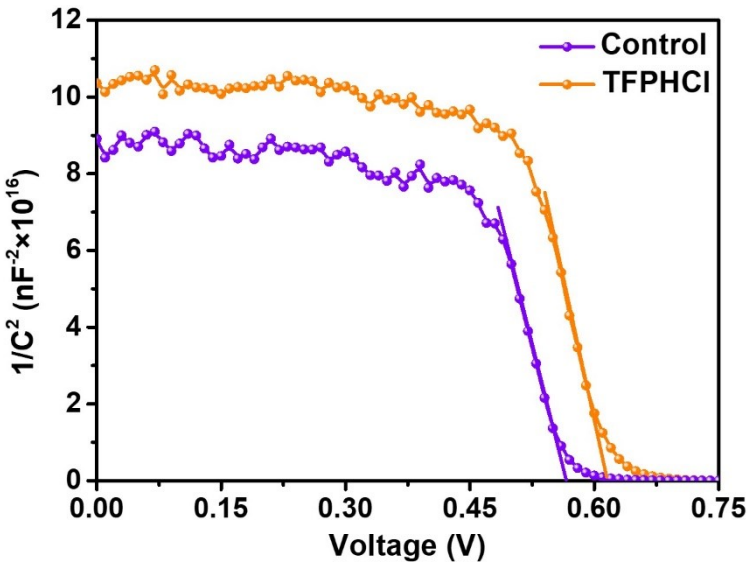

Figure S23. Mott-Schottky analysis of control and TFPHCl-modified NBG devices.

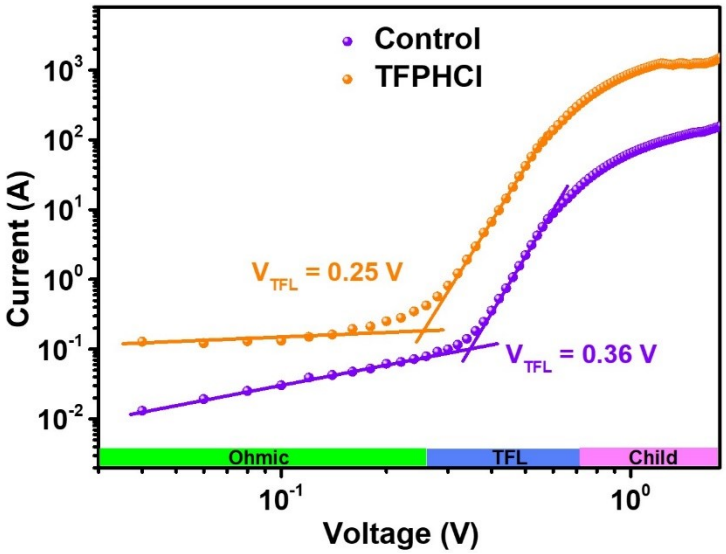

Figure S24. Dark *J-V* of electron-only devices based on NBG perovskite films w/o and with TFPHCl.

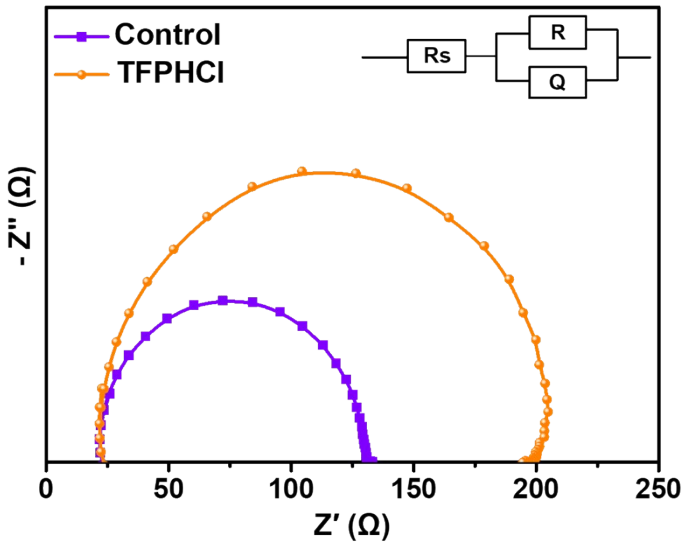

Figure S25. Nyquist plots of control and TFPHCl-modified NBG devices.

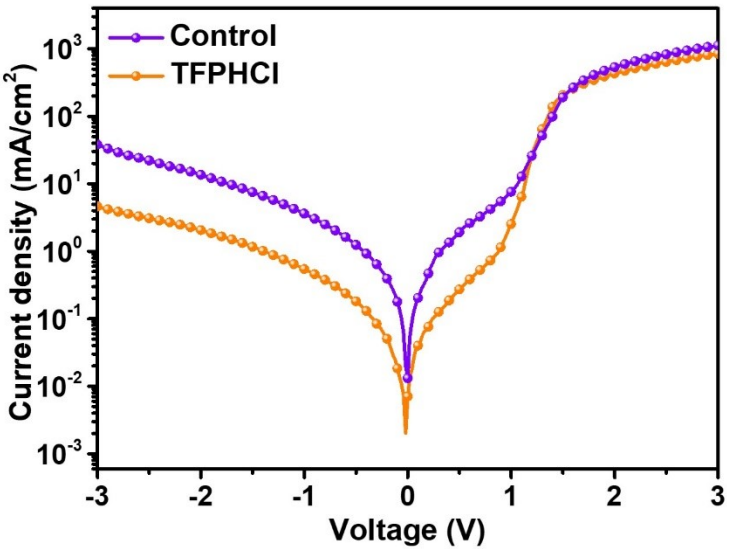

Figure S26. Dark *J-V* curves of control and TFPHCl-modified NBG devices.

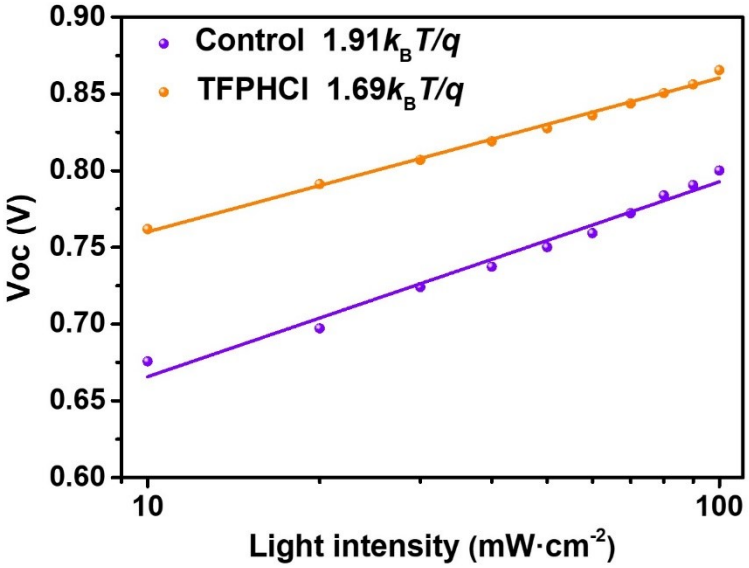

Figure S27. Dependence of control and TFPHCl-modified NBG devices at various illumination intensities.

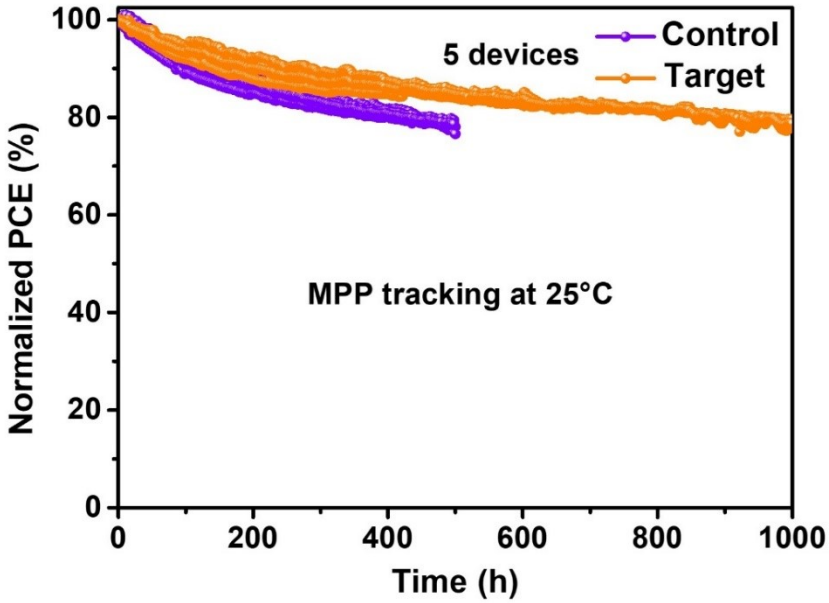

Figure S28. MPP stability tracking of five independent control and TFPHCl-modified NBG devices at 25 °C under continuous illumination.

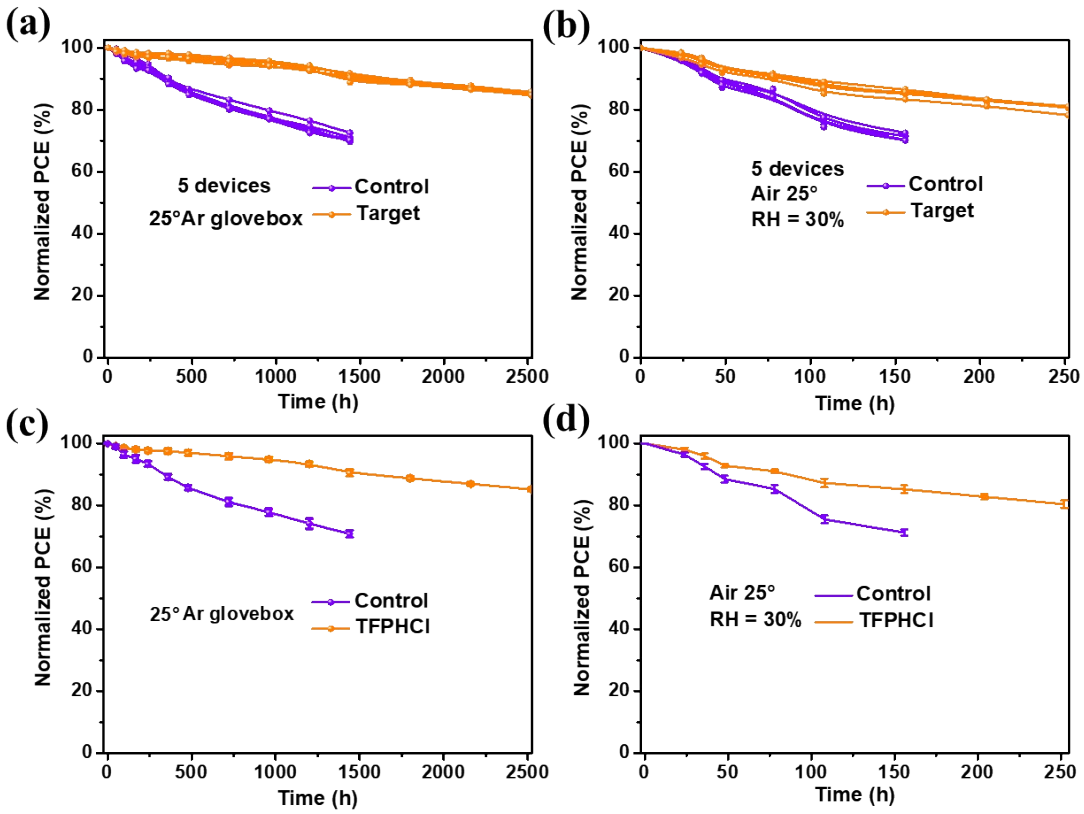

Figure S29. The long-term stability of five devices and averages for control and TFPHCl-modified NBG devices stored in (a, c) Ar glovebox and (b, d) air (RH = 30%).

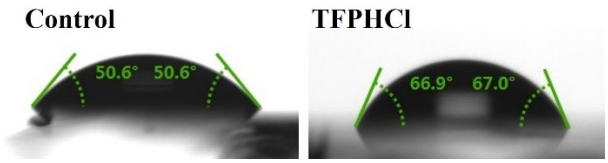

Figure S30. Water contact angle measurement on NBG perovskite films w/o and with THPHCl.

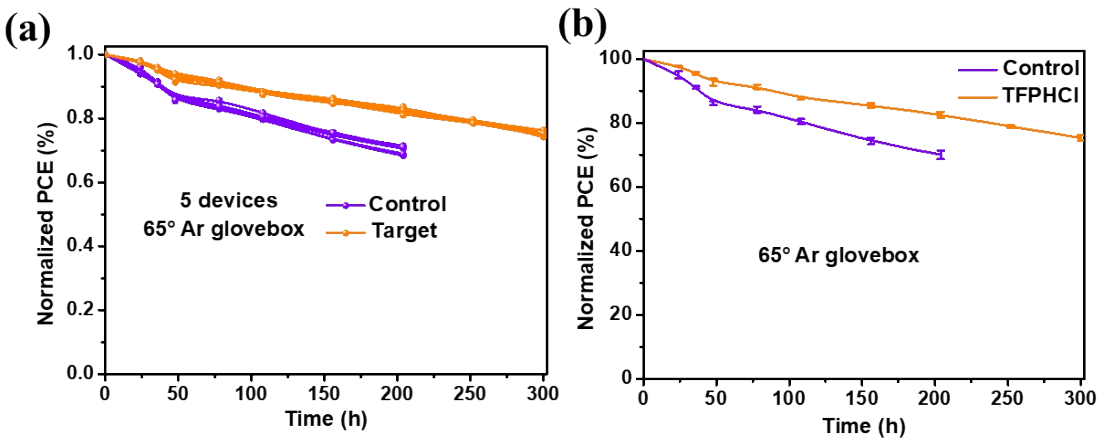

Figure S31. The long-term stability of (a) five devices and (b) averages for control and TFPHCl-modified NBG devices stored at 65° heating (Ar glovebox).

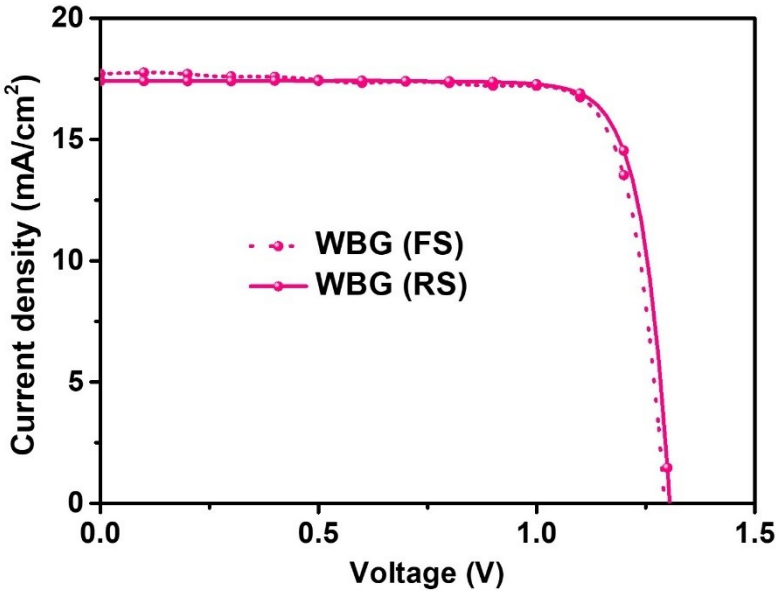

Figure S32. *J-V* curves of control WBG perovskite device.

The design and optimisation for WBG subcell are as follows: Self-assembled monolayers (SAMs) have become most popular hole transport materials in p-i-n PSCs. There is a bidentate bonding interaction between SAM and ITO, whereas tridentate bonding interaction between SAM and NiOx[5,6]. Besides, Me-4PACz features more suitable HOMO and better energy level matching with WBG perovskite. Therefore, device structure for WBG subcells designed as ITO/NiOx/SAM/WBG/C_{60}/BCP/Ag. Moreover, recent reports suggested that V_{oc} loss mainly stems from the relatively low radiative efficiency of bulk absorber and severe nonradiative recombination at the interface between WBG perovskite and charge-transport layers, rather than from halide segregation[7,8]. Therefore, it is important to modify the bulk and surface of WBG perovskites for higher V_{oc} and hence better performance. Here, 1,3-Propyldiammonium diiodide was dissolved in IPA for post-process passivation of WBG perovskkite films, which effectively improved WBG device performance.

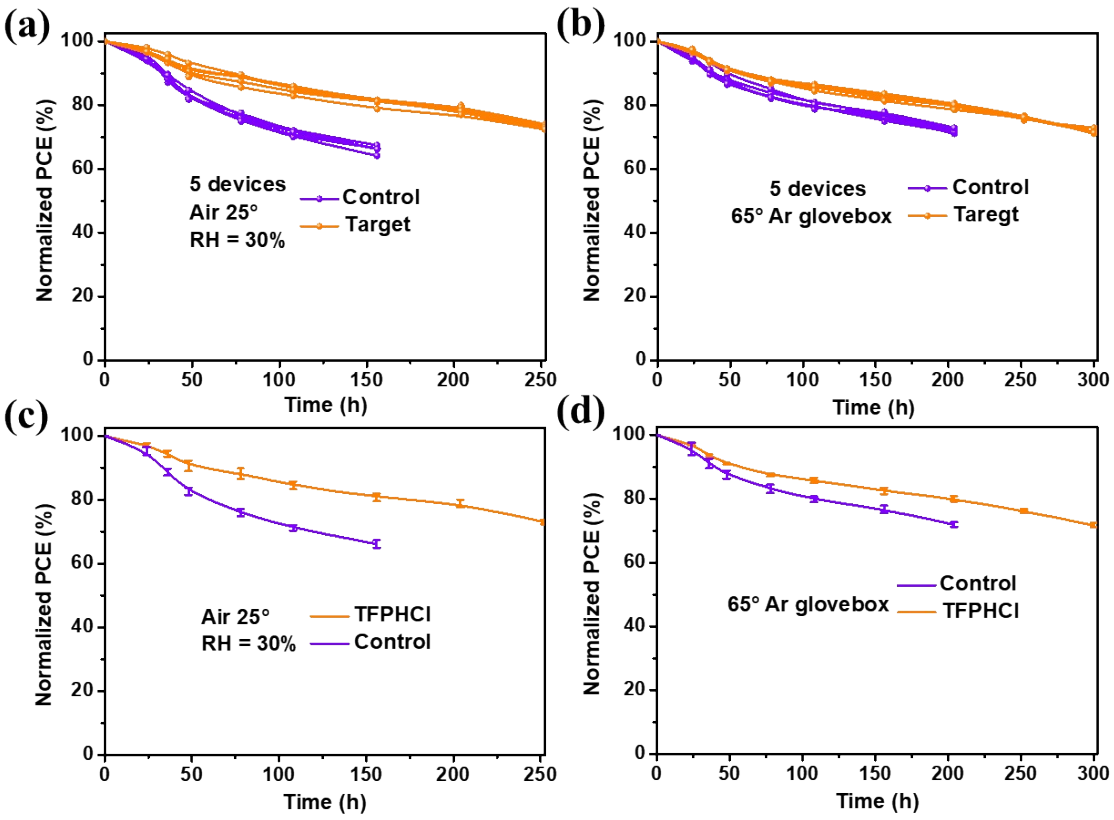

Figure S33. The long-term stability of five devices and averages for control and TFPHCl-modified tandem devices stored in (a, c) air (RH = 30%) and (b, d) 65° heating (Ar glovebox).

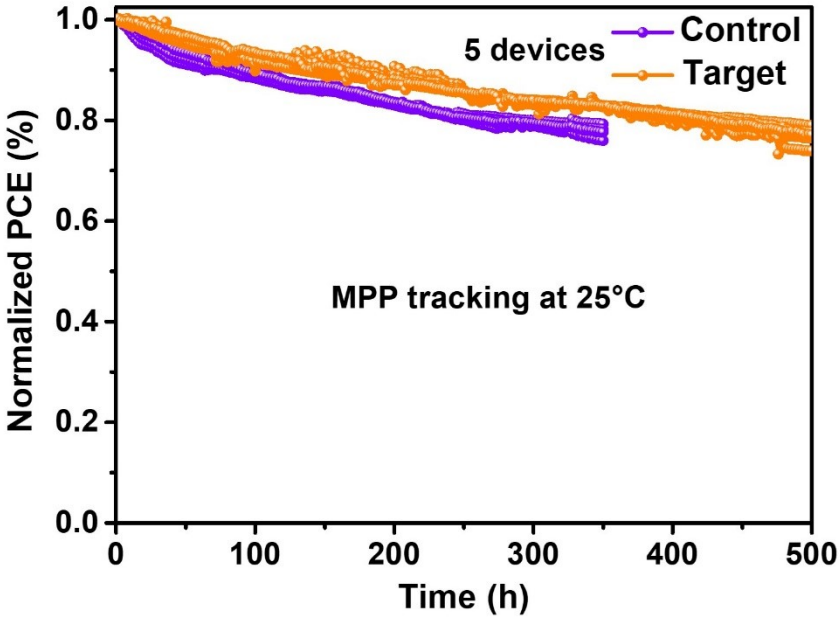

Figure S34. MPP stability tracking of five independent control and TFPHCl-modified all-perovskite tandem devices at 25 °C under continuous illumination.

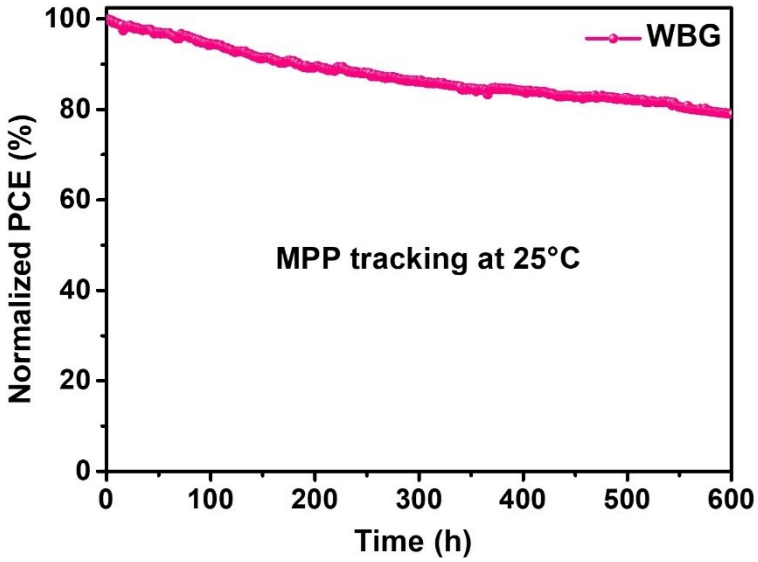

Figure S35. MPP stability tracking for WBG device at 25 °C under continuous illumination.

Table S1. Contact angle and surface energy for NBG perovskite films w/o and with TFPHCl.

Perovskite	contact angle (θ)		surface energy (mJ/m^2)		
	diiodomethane	glycerol	σ_s^d	σ_s^p	total
Control	20.5	49.0	47.63	7.84	55.47
TFPHCl	35.1	72.0	41.87	1.82	43.69

According to Owens-Wendt method, total surface energy of NBG perovskite film (σ_S) can be calculated by the following equation[9-11]:

$$\sigma_S = \sigma_s^d + \sigma_s^p \tag{5}$$

$$\sqrt{\sigma_l^d * \sigma_s^d} + \sqrt{\sigma_l^p * \sigma_s^p} = \frac{\sigma_l(1+\cos\theta)}{2} \tag{6}$$

$$\sigma_s^d = \frac{\sigma_l(1+\cos\theta)^2}{4} \tag{7}$$

where σ_s^d and σ_s^p denote dispersive and polar components of surface energy for NBG perovskite film, respectively, while σ_l^d and σ_l^p denote dispersive and polar components of surface tension of the liquid, respectively. σ_l denote total surface tension of the liquid.

Notably, this case adopted diiodomethane and glycerol as solvents for contact angle test. The surface tension of diiodomethane has no polar component, which implicating $\sigma_l = \sigma_l^d$ = 50.8 mN/m and equation 2 can be simplified to equation 3. Combined with the contact angle result (diiodomethane), σ_s^d can be calculated. For glycerol, σ_l^p and σ_l^d are 37.0 mN/m and 26.4 mN/m, respectively.

Table S2. Summary of PL decay lifetime for NBG perovskites w/o or with charge extraction layers.

Perovskite	τ_{pvk} (ns)	τ_{pedot} (ns)	τ_{C60} (ns)	d (nm)	L_D (e^-) (nm)	L_D (h^+) (nm)
Control	499	40.1	64.7	800	1866	2437
TFPHCl	1649	31.6	48.8	800	4126	5155

PL lifetime curves were fitted by the double exponential formula (2) and the average carrier lifetime was calculated by the following formula (3). Finally, the diffusion length could be expressed according to formula (4)[12,13].

$$I(t) = A_1 \exp\left(-\frac{t}{\tau_1}\right) + A_2 \exp\left(-\frac{t}{\tau_2}\right) + I_0 \tag{8}$$

$$\tau_{avg} = \frac{A_1\tau_1^2 + A_2\tau_2^2}{A_1\tau_1 + A_2\tau_2} \tag{9}$$

$$L_D \approx \frac{2d}{\pi}\sqrt{2\left(\frac{\tau_{avg}}{\tau_{quench}} - 1\right)} \tag{10}$$

Table S3. Parameters of the UPS spectra for NBG perovskite films w/o and with TFPHCl.

Perovskite		E_c	E_v	E_F
Control	top	4.00	5.25	4.76
	bottom	3.99	5.24	4.75
TFPHCl	top	4.03	5.28	4.67
	bottom	4.00	5.25	4.73

Table S4. Summary of the photovoltaic parameters of NBG devices with different concentration TFPHCl.

Perovskite	V_{oc} (V)	FF (%)	J_{sc} (mA/cm^2)	PCE (%)
0 mg/ml	0.83	76.95	32.79	21.09
1 mg/ml	0.85	78.40	33.12	22.00
2 mg/ml	0.88	79.15	33.11	23.09
3 mg/ml	0.86	77.77	32.64	21.82
4 mg/ml	0.83	77.71	31.61	20.38

Table S5. Photovoltaic parameters of 20 devices based on control NBG devices.

No.	V_{oc} (V)	FF (%)	J_{sc} (mA/cm^2)	PCE (%)
1	0.84	76.39	32.63	21.00
2	0.83	76.19	32.92	20.88
3	0.84	75.87	32.58	20.97
4	0.83	76.95	32.79	21.09
5	0.80	76.93	32.05	19.87
6	0.83	75.89	32.59	20.72
7	0.83	74.82	32.75	20.39
8	0.81	77.82	32.43	20.43
9	0.81	76.03	32.96	20.38
10	0.83	73.35	32.52	19.94
11	0.83	75.77	32.81	20.80
12	0.81	78.05	31.53	19.98
13	0.81	76.14	32.16	19.96
14	0.82	76.25	32.64	20.40
15	0.81	72.92	32.54	19.26
16	0.82	72.00	32.74	19.44
17	0.79	74.84	32.89	19.48
18	0.83	73.98	32.73	20.13
19	0.84	76.10	31.97	20.44
20	0.84	75.57	32.03	20.88
Average	0.82±0.014	75.59±1.553	32.51±0.378	20.32±0.551

Table S6. Photovoltaic parameters of 20 devices based on TFPHCl-modified devices.

No.	V_{oc} (V)	FF (%)	J_{sc} (mA/cm^2)	PCE (%)
1	0.88	79.15	33.11	23.09
2	0.86	76.52	33.73	22.30
3	0.87	77.93	33.65	22.74
4	0.87	77.52	34.01	22.99
5	0.87	79.29	33.31	22.93
6	0.87	77.93	33.65	22.74
7	0.86	79.52	33.03	22.71
8	0.86	78.11	33.09	22.45
9	0.87	79.06	32.84	22.46
10	0.86	77.45	33.37	22.29
11	0.86	78.73	33.79	23.01
12	0.87	78.41	33.66	22.92
13	0.87	79.07	33.30	22.87
14	0.86	78.23	32.99	22.30
15	0.87	77.03	33.45	22.36
16	0.87	76.94	32.91	21.94
17	0.87	77.96	32.27	21.97
18	0.86	76.58	33.88	22.37
19	0.86	78.10	32.54	21.91
20	0.87	76.22	33.17	21.99
Average	0.86±0.005	77.99±0.982	33.28±0.454	22.51±0.388

Table S7. Summary of the photovoltaic parameters of NBG devices of $FA_{0.6}MA_{0.3}Cs_{0.1}Pb_{0.4}Sn_{0.6}I_3$ with different concentration TFPHCl.

Perovskite	V_{oc} (V)	FF (%)	J_{sc} (mA/cm^2)	PCE (%)
0 mg/ml	0.82	76.19	32.84	20.49
1 mg/ml	0.85	77.81	32.73	21.64
2 mg/ml	0.86	79.41	32.69	22.41
3 mg/ml	0.84	77.30	32.86	21.38

Table S8. Summary of the photovoltaic parameters of NBG devices of $(FA_{0.9}EA_{0.1})_{0.98}EDA_{0.01}SnI_3$ with different concentration TFPHCl.

Perovskite	V_{oc} (V)	FF (%)	J_{sc} (mA/cm^2)	PCE (%)
0 mg/ml	0.78	71.45	19.99	11.27
1 mg/ml	0.82	74.29	19.82	12.05
3 mg/ml	0.84	76.94	20.59	13.27
5 mg/ml	0.82	69.92	19.99	11.60

Table S9. Photovoltaic performance of WBG perovskite devices.

Device	Scan	V_{oc} (V)	FF (%)	J_{sc} (mA/cm^2)	PCE (%)
WBG	forward	1.29	80.46	17.70	18.43
	reverse	1.30	82.27	17.40	18.69

Table S10. Photovoltaic performance of all-perovskite tandem devices.

Device	Scan	V_{oc} (V)	FF (%)	J_{sc} (mA/cm^2)	PCE (%)
Control	forward	2.04	77.53	15.61	24.69
	reverse	2.05	78.66	15.56	25.14
TFPHCl	forward	2.10	82.25	15.76	27.18
	reverse	2.11	83.08	15.64	27.42

Reference:

1. G. Yan, G. Sui, We. Chen, K. Su, Y. Feng, B. Zhang, *Chem. Mater*., 2022, **34**, 3346-3356
2. X. Zhang, H. Liu, W. Wang, J. Zhang, B. Xu, K. Karen, Y. Zheng, S. Liu, S. Chen, K. Wang, X. Sun, *Adv. Mater.* 2017, **29**, 1606405.
3. L. Ji, X. Zhang, T. Zhang, Y. Wang, F. Wang, Z. Zhong, Z. Chen, Z. Xiao, L. Chen, S. Li, *J. Mater. Chem. A*, 2019, **7**, 9154-9162.
4. Y. Tian, W. Yue, L. Tian, H. Cai, X. Zhu, J. Zhao, J. Xiao, Y. Cheng, J. Zhong, *Energy Technol.*, 2023, **11**, 2300454.
5. M.A. Truong, T. Funasaki, L. Ueberricke, W. Nojo, R. Murdey, T. Yamada, S. Hu, A. Akatsuka, N. Sekiguchi, S. Hira, L. Xie, T. Nakamura, N. Shioya, D. Kan, Y. Tsuji, S. Iikubo, H. Yoshida, Y. Shimakawa, T. Hasegawa, Y. Kanemitsu, T. Suzuki, A. Wakamiya*, J. Am. Chem. Soc.*, 2023, **145**, 7528-7539.
6. Z. Li, X. Sun, X. Zheng, B. Li, D. Gao, S. Zhang, X. Wu, S. Li, J. Gong, J.M. Luther, Z. Li, Z. Zhu, *Science*, 2023, **382**, 284-289.
7. S. Mahesh, J. M. Ball, R. D. J. Oliver, D. P. McMeekin, P. K. Nayak, M. B. Johnston H. J. Snaith, *Energy Environ. Sci.*, 2020, **13**, 258-267.
8. X. Zheng, A. Y. Alsalloum, Y. Hou, E. H. Sargent, O. M. Bakr, ACS Cent. Sci., 2023, 9, 14-26.
9. S. Nuriel, L. Liu, A.H. Barber, H.D. Wagner, *Chem. Phys. Lett.*, 2005, **404**, 263-266A.
10. A. Michiardi, C. Aparicio, B.D. Ratner, J.A. Planell, J. Gil, *Biomaterials*, 2007, **28**,

586-594.

11. X. Meng, Y. Wang, J. Lin, X. Liu, X. He, J. Barbaud, T. Wu, T. Noda, X. Yang, L. Han, *Joule*, 2020, **4**, 902-912.
12. P. Li, X. Liu, Y. Zhang, C. Liang, G. Chen, F. Li, M. Su, G. Xing, X. Tao, Y. Song, *Angew. Chem. Int. Ed.*, 2020, **59**, 6909-6914.
13. G. Kim , H. Min , K. Lee , D. Lee , S. Yoon, S. Seok, *Science*, 2020, **370**, 108-112.

data.zip